Chinese Journal of
POLYMER SCIENCE

RESEARCH ARTICLE

https://doi.org/10.1007/s10118-026-3773-8
Chinese J. Polym. Sci.

Self-crosslinking Waterborne Polyurethane with Antibacterial Performance and Solvent-free Adhesiveness

Shan-Shan Li, Sang-Qi Chen, Yi Xiao, Wen-Jie Xu, and Xing-Huan Lin*

College of Chemistry and Materials Science, Gannan Normal University, Ganzhou 341000, China

Electronic Supplementary Information

Abstract Waterborne polyurethanes (WPUs) are increasingly valued for their low volatile organic compound emissions but suffer from poor water resistance and weak mechanical properties. Herein, a strategy based on covalent self-crosslinking combined with ionic crosslinking was proposed to construct a PU elastomer with excellent water resistance and antibacterial activity. This film exhibited dramatically enhanced tensile strength (12.7 MPa) and toughness (43.0 MJ/m^3), far exceeding those of non-crosslinked and single-crosslinked PU films. Notably, the chain segments with C=O and N−H bonds assembled into hard-phase regions, enabling efficient energy dissipation through the rupture and reformation of reversible H-bonds. This WPU can serve as a recoverable, solvent-free adhesive, achieving lap shear strengths of 2.69 MPa (glass). Moreover, the excellent water resistance of WPU materials ensures a sustained high adhesion strength under wet conditions. In addition, the chlorinated film demonstrated satisfactory cytocompatibility and antibacterial efficiency. This high-performance and sustainable PU material holds great promise for biomedical applications.

Keywords Waterborne polyurethane; Self-crosslinking; Antibacterial; Cell compatibility; Adhesive

Citation: Li, S. S.; Chen, S. Q.; Xiao, Y.; Xu, W. J.; Lin, X. H. Self-crosslinking waterborne polyurethane with antibacterial performance and solvent-free adhesiveness. *Chinese J. Polym. Sci.* https://doi.org/10.1007/s10118-026-3773-8

INTRODUCTION

Compared with solvent-borne polyurethanes, waterborne polyurethanes (WPUs) offer unique environmental advantages owing to their minimal emission of volatile organic compounds (VOC).[1,2] The hydrophilicity of WPU is improved by incorporating hydrophilic components, such as dimethyl propionic acid, which, upon neutralization, yields a stable self-emulsified emulsion. However, the presence of such hydrophilic groups often compromises the water resistance of WPU. Furthermore, in contrast to solvent-borne polyurethanes, WPUs typically exhibit inherent deficiencies in their mechanical properties, thereby limiting their practical applications. In recent years, considerable effort has been devoted to improving the mechanical performance of WPUs. There are various effective strategies, including physical blending with optimized nanofillers,[3] introduction of diverse H-bonds,[4,5] ionic interactions,[6,7] and metal-ligand coordination.[8,9] Among these, the incorporation of diverse H-bonds has been widely exploited to construct WPU films with high mechanical performance and self-healing capability because of the directionality and stability of H-bonds.[10–12] Nevertheless, an increase in H-bonds might further compromise the water resistance of WPU materials because polar hydrogen bonds are inherently more hydrophilic than polyester or polyether soft segments.[13] Moreover, PUs with inadequate water resistance can provide favorable conditions for microorganism growth and proliferation, leading to mildew formation and a consequent decline in serviceability.[14]

To overcome these limitations, one promising approach involves enhancing the water resistance of WPU materials by physically blending hydrophobic compounds or introducing hydrophobic segments into the WPU macromolecular chain, such as fluorinated compounds.[15–18] However, fluorinated compounds cannot degrade in the environment and may accumulate in living organisms. In recent years, the introduction of organic/inorganic silicon compounds has been widely explored to improve the water resistance of WPU materials owing to their intrinsic hydrophobicity, nontoxicity, and environmental friendliness.[19,20] Among these, reactive siloxanes such as 3-aminopropyl trimethoxysilane (APTMS) can serve as effective crosslinkers for polyurethanes. Covalent crosslinked PUs offer the dual benefits of improved water resistance and enhanced mechanical properties. Furthermore, to mitigate mildew formation in WPU materials, an effective strategy is to construct molecular structures with antimicrobial properties.[7,21,22] To date, most reported antibacterial WPUs have been designed and synthesized *via* the incorporation of quaternary ammonium salts (QAS).[23–25] However, the antibacterial efficacy of QAS-functionalized materials often falls short of practical requirements because of their moderate an-

* Corresponding author, E-mail: Linxinghuan@gnnu.edu.cn
Received April 29, 2026; Accepted June 6, 2026; Published online September 10, 2026

timicrobial activity. In contrast, *N*-halamine, as a prominent organic halogen-based antibacterial agent, offers distinct advantages over other antimicrobial systems, including powerful antibacterial activity, broad antibacterial spectrum, and antibacterial renewability.[26] For example, Sun *et al*. prepared antimicrobial PU materials by covalently grafting 5,5-dimethylhydantoin (DMH) onto polyurethane surfaces.[27] Nevertheless, this approach is hindered by drawbacks, such as cumbersome procedures and the use of organic solvents. In our previous work, novel *N*-halamine-functionalized antibacterial WPUs were successfully designed and synthesized using introducing 3-(2,3-dihydroxypropyl)-5,5-dimethylimidazolidine-2,4 dione as chain extenders.[28,29] These antibacterial WPUs have been applied as functional coatings on various fabrics.[29]

In addition to functional coatings, WPUs have aroused increasing interest for a wide range of applications, such as foams,[30] synthetic skin,[31] and adhesives[32] to maintain sustainable development. Despite notable advancements in WPU-based adhesives in recent years, their widespread application remains constrained by inadequate water resistance and low bonding strength, especially in gluing metal substrates. Generally, an adhesive bond strength on metal substrates exceeding 1 MPa is considered high-strength bonding.[32] Moreover, compared to volatile solvents such as acetone, water evaporates quite slowly, often requiring several days in typical bonding processes. Consequently, solvent-free adhesives are attractive alternatives. Recently, reversible adhesives capable of debonding and re-bonding with substrates have attracted considerable interest.[33,34] Solvent-free adhesives that combine high bonding strength with reusability hold significant promise for emerging applications. Nonetheless, achieving solvent-free adhesives with strong adhesion and simultaneous reusability remains a formidable challenge.

Herein, after rational structural design, a self-crosslinkable waterborne polyurethane was synthesized, which was capable of forming a crosslinked network *via* Si—O—Si covalent bonds. Subsequently, a series of polyurethane films with excellent mechanical properties, water resistance, and antibacterial performance were fabricated by casting the PU solution and immersing it in $CaCl_2$ solution to introduce ionic crosslinking, followed by drying and chlorination. Driven by multiple H-bonds, the PU films presented phase-separated structures, wherein hard-phase regions were formed by the aggregation of H-bonds from the hard segments, while the soft-phase regions were composed of soft segments. The introduction of Si—O—Si covalent crosslinks between macromolecular chains substantially enhances the mechanical properties, thermal stability, and water resistance of the WPU material. The hard-phase regions contribute to energy dissipation through the reversible formation and dissociation of multiple hydrogen bonds, resulting in PU films with high mechanical strength and toughness. The reversibility of these H-bonds enabled the reformation of hard-phase regions upon the heating-cooling process, imparting a PU adhesive with high bonding strength and reusability. As demonstrated in this study, the adhesive performed effectively across a wide temperature range and in humid environments, broadening its potential applications in various fields as a promising adhesive. To further explore the biomedical potential of the PU film as a scaffold, the antibacterial efficacy and cytotoxicity of the chlorinated PU films were evaluated. The films exhibited excellent antibacterial activity and satisfactory cell compatibility.

EXPERIMENTAL

Materials

Polybutylene adipate, ethylene glycol ester diol (PEBA-1000) were supplied by Shanghai Gaoqiao Chemical Co., Ltd. Isophorone diisocyanate (IPDI) was obtained from Bayer (Germany). Dimethylolpropionic acid (DMPA), dibutyl tin dilaurate (DBTDL) were purchased from Anaiji Chemical Co., Ltd. 3-aminopropyltrimethoxysilane (APTMS) was purchased from Aladdin Chemical Co., Ltd. 3-(2,3-dihydroxypropyl)-5,5-dimethylimidazolidine-2,4 dione (Hydantoin diol, HD) was synthesized according to the previous work.[29] Other chemical agents were purchased from Sinopharm Chemical Reagent Co., Ltd.

Synthesis Pathway of PUs

The synthesis pathway for self-crosslinkable waterborne polyurethanes is shown in Fig. 1(a). In step 1, a certain amount of PEBA (M_n: 1000) was placed in a four-necked flask, and a small amount of water in PEBA was removed by vacuum depression vaporization at 120 °C for 3 h. Then, a certain amount of IPDI was added when the temperature was cooled to 90 °C and the mixture was stirred for 40 min. In step 2, DMPA and three drops of DBTDL as a catalyst were added, and the reaction continued for 4 h at 90 °C. Subsequently, the reaction temperature was reduced to 60 °C, a certain amount of HD was added, and the reaction continued for 2 h (step 3). Different amounts of APTMS were added and the reaction was continued for 1 h at 60 °C (step 4). Afterward, TEA was added to neutralize the above DMPA, and the reaction continued for 30 min when the temperature was reduced to 40 °C (step 5). Finally, a certain amount of water was added dropwise under a mechanical stirring speed of 1000 r/min to form the WPU emulsions. To ensure an anhydrous environment, all reaction processes were carried out under a nitrogen atmosphere, and the reaction progress was monitored using the di-*N*-butylamine-toluene titration method. A spot of acetone should be added when the viscosity of the products is extremely high, and the acetone should be removed by vacuum depression vaporization at 35 °C finally. The PU emulsions could be stored for more than 6 months with a solid content of 50%. The synthesized PU was sequentially denoted as PU*x*, where *x* (0, 1, 2, 3, or 5) is the mass ratio of APTMS. The detailed components of PU*x* are listed in Table S1 in the electronic supplementary information (ESI).

Preparation of PU Films

A certain amount of the WPU emulsion was poured onto the glass plates. Subsequently, the WPU emulsions on glass plates were placed into a $CaCl_2$ solution for 5 h. Afterward, the glass plates were removed and washed thoroughly with deionized water. All samples were dried in air for 1 day and then in an oven at 60 °C for 2 days to induce the formation of a Si—O—Si covalent crosslinking network within the polyurethane films. After drying, the PU films obtained without dipping in $CaCl_2$ solu-

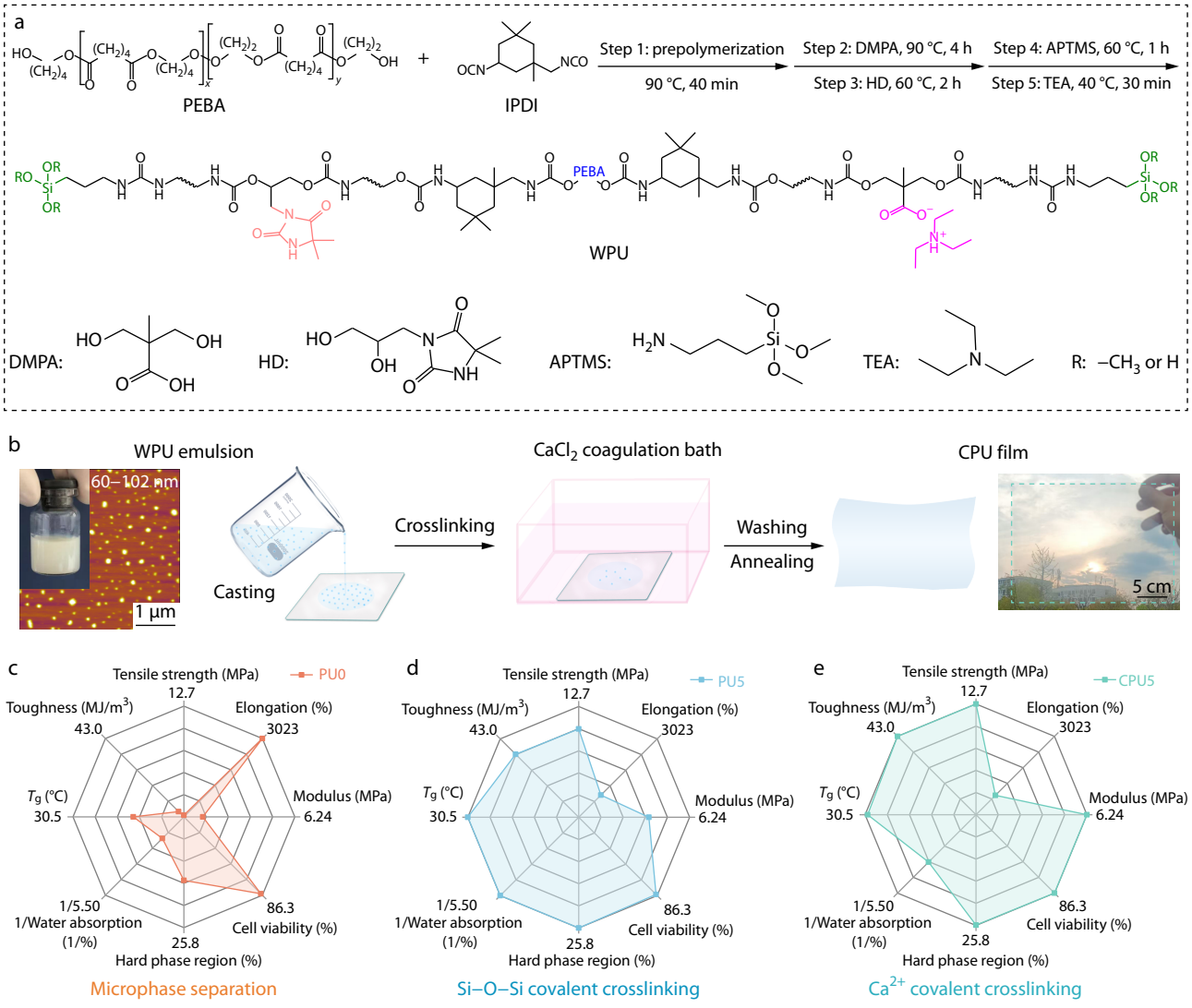

Fig. 1 Synthesis of WPUs and preparation of CPU films. (a) Synthesis pathway of WPUs; (b) Preparation of PU film from WPU emulsion; Radar plots comparing physicochemical properties and bioactivities of (c) PU0, (d) PU5 and (e) CPU5 films.

tion were designated as PU*x* films, where *x* (0, 1, 2, 3, or 5) represents the mass ratio of APTMS. The PU*x* crosslinked with a 5% $CaCl_2$ solution was identified as CPU*x* (CPU1, CPU2, CPU3, and CPU5). The thicknesses of the films were approximately 0.3 mm.

Chlorination and Chlorine Content Measurement

First, chlorinated samples were obtained by immersion in dilute NaClO solution (pH is about 7) at ambient temperature for 1 h. The chlorinated films were fully washed 3 times with deionized water and dried in an oven at 45 °C for 1 h to remove free chlorine. The active chlorine (Cl^+) on the chlorinated WPU films was fully released in an acetic acid/ethanol solution (*V*:*V*, 1:9) for 1 h. Cl^+ content was measured using a modified iodometric/thiosulfate titration method. The Cl^+ contents of the WPU films were calculated using the following equation:

$$Cl^+ \text{ content } (\%) = \frac{N \times (V_0 - V_1) \times 35.45}{2W} \times 100 \quad (1)$$

where Cl^+ content (%) is the weight percent of active chlorine on the sample, *N* is the normality (equiv/L), V_0 and V_1 are the volumes (L) of the $Na_2S_2O_3$ solution before and after titration, respectively, and *W* is the weight (g) of chlorinated WPU films.

Characterization

The ^{1}H-NMR spectra of PU0 and PU5 were recorded on an AVANCE 400 MHz spectrometer (Bruker, Germany). The particle size and particle distribution index (PdI) of the PUs emulsions were tested at 25 °C using a Malvern Zetasizer Nano model ZS90 instrument with a 90° scattering angle. The optical transmittance of the WPU films was measured using a UV-Vis spectrometer (UV-6, Shanghai Meipuda Instrument Co., Ltd., China) in the wavelength range of 900–200 nm. The FTIR spectra of the PU films were obtained using a Thermo Nicolet Fourier transform infrared spectrometer (Thermo Fisher, Waltham, MA, USA) with a scanning range of 4000–500 cm^{-1} and a resolution of 32 scans. The X-ray diffraction (XRD) patterns of the PU films were recorded using a Rigaku Smartlab 9000 diffractometer in the reflection mode at a scanning speed of 5 (°)/min at 200 mA and 45 kV. Raman spectroscopy of the PU films was performed using a Raman imaging microscope (Thermo Scientific DXR xi, USA) with an excitation laser wavelength of 532 nm and a spatial resolution for Raman mappings of 200 nm. The collected spectra were

preprocessed using cosmic ray removal, noise filtering, and normalization techniques. The proportion of different domains was calculated using the multivariate curve resolution (MCR) method, which was developed using the OMNICxi software. The surface morphologies of the films were characterized using scanning electron microscopy (SEM, Zeiss, SIGMA, Germany). The SEM was equipped with an energy dispersive X-ray spectrometer (EDS, ULTIM MAX, OXFORD Instruments, UK) to detect the surface elemental composition of the films. X-ray photoelectron spectroscopy (XPS, ESCALAB250Xi, Thermo Fisher Scientific, USA) was performed using a Kratos XSAM800 X-ray photoelectron spectrometer. Dynamic mechanical analysis (DMA) of PU films (the length of 1 cm and the thickness of 0.3 mm) was performed in "multi-frequency-strain" mode by a TA Q800 instrument under a nitrogen atmosphere. The frequency was 1 Hz, and temperature range was from –60 °C to 100 °C at a heating rate of 5 °C/min. Thermogravimetric analysis (TG) of the films was performed using a Pyrisdiamond TA Lab System (PerkinElmer) under a nitrogen atmosphere. The temperature range was from 40 °C to 560 °C at a heating rate of 10 °C/min.

Mechanical Properties

The tensile properties of the PU films were measured using a universal tensile tester (INSTRON Instrument, Model 5576, USA) at a speed of 50 mm/min, according to ASTM D638. The toughness and Young's modulus were calculated from the tensile stress-strain curves. The cyclic tensile properties of PU films were tested at room temperature. The cycle tensile of the PU film with increasing strain, but no resting time, was tested until the films fractured. The PU film was further stretched to 200% in successive loading-unloading cycles with no resting time for 10 cycles. Subsequently, the cycle tensile strength of the PU film was tested with a resting time of 5 min and 2 h to evaluate the recovery of the strain. The hysteresis loops of the film were calculated from each full region of the stress-strain curves.

Antibacterial Efficacy and Cell Compatibility

The antibacterial efficiencies of the samples before and after chlorination against *Staphylococcus aureus* (*S. aureus*, ATCC 6538, about $6.15\times10^6\pm0.09\times10^6$ CFU/sample) and *Escherichia coli* (*E. coli*, ATCC 15597, approximately $1.57\times10^7\pm0.26\times10^7$ CFU/sample) were assessed using a 'sandwich' model. Bacterial suspensions (20 μL) were placed between two pieces of PU films (1.5 cm × 1.5 cm). After incubation at 37 °C, the samples were quenched with sodium thiosulfate solution (5.0 mL, 0.02 N). Subsequently, the films were immersed in a PBS solution, and the solution was vortexed to transfer bacteria from the films to the PBS solution. The PBS solution containing bacteria was diluted several times (10-fold each time) using a sterilized PBS solution. The 10 μL of each bacterial dilution was placed onto an agar plate, and the agar plates were incubated at 37 °C for 24 h. Finally, the bacterial colonies were counted to calculate the bacterial survival rate. The cell compatibility of the WPU films was evaluated using L929 cells according to the International Standard Organization (ISO/EN 10993-5) and reported work.[35]

Adhesion Properties

A PU adhesive (thickness: 0.3 mm was cut into strips (20 mm × 5 mm), and one strip was sandwiched between two pieces of substrates. The substrates were then gently pressed and clamped using a clip. Subsequently, the substrates were heated to different temperatures in an oven for 20 min and then cooled to room temperature. The lap-shear strength was measured using a universal tensile tester (INSTRON Instruments, Model 5576, USA) at a speed of 5 mm/min. Each sample was analyzed at least three times. Glass and tin plate plates were used as substrates in this study.

RESULTS AND DISCUSSION

Design Strategy and Characterizations

A series of self-crosslinkable waterborne polyurethanes (WPUs) were synthesized by rational molecular design (Fig. 1a and Fig. S1 in ESI). First, the prepolymer was synthesized by reacting excess isophorone diisocyanate (IPDI) with PEBA. Subsequently, chain extenders, dimethylolpropionic acid (DMPA) as the hydrophilic component, and hydantoin diol (HD) as the antibacterial chain extender, were introduced to yield PU0, which lacked Si—O—Si covalent crosslinking. To impart self-crosslinking capability, 1 wt%–5 wt% of 3-aminopropyltrimethoxysilane (APTMS) was carefully selected as an end-capping reagent to prepare–PU1-PU5. The structure of WPU was characterized by ^{1}H-NMR, and representative data for PU0 and PU5 are shown in Fig. S2 (in ESI). During emulsion formation under mechanical stirring, the methoxy groups along the polymer chains were susceptible to hydrolysis, generating hydroxyl groups. The WPU macromolecular chains self-assembled into approximately spherical droplets (AFM image, Fig. 1b), with hydrophobic silicon-containing segments (depicted in red in Fig. S3 in ESI), likely encapsulated by hydrophilic carboxyl-bearing chains. The resulting emulsions exhibited average particle sizes ranging from 60 nm to 102 nm, with polydispersity index (PdI) between 0.06 and 0.10 (Fig. S4 in ESI). Notably, no significant agglomeration or precipitation was observed even after more than 6 months of storage (Fig. 1b). This molecular design strategy not only afforded enabled the formation of stable WPU emulsions but also endowed the polymer chains with self-crosslinking capabilities.

Furthermore, ionic crosslinking was introduced to enhance the mechanical performance of the PU films. As shown in Fig. 1(b), the WPU emulsion was cast onto a glass plate and subsequently immersed in $CaCl_2$ solution to induce regeneration and crosslinking. During this process, the emulsion gradually demulsified in the $CaCl_2$ solution, accompanied by a color change from bluish to colorless (Fig. S5 in ESI), driven by the self-assembly of the molecular chains. Specifically, the carboxylic groups along the polymer chains coordinate with the Ca^{2+} ions to form Ca—$(COO)_2$ structures, leading to progressive demulsification. After washing, the PU films were annealed at 60 °C. In addition to removing water, this post-curing stage provides sufficient thermal energy to promote the condensation of silanol groups (Si—OH) derived from APTMS hydrolysis, thereby facilitating the formation of a robust Si—O—Si covalent crosslinking network.[36] The resulting transparent crosslinked PU (denoted as CPU) films were obtained, exhibiting transmittance values between 79.6% and 86.6% at 550 nm (Fig. S6 in ESI).

As illustrated in Figs. 1(c)–1(e) and Table S2 (in ESI), the PU0 film displayed a microphase-separated structure consisting of a small fraction of hard phase regions (rich H-bond regions) and a large proportion of flexible molecular segments. This architecture resulted in a low glass transition temperature (T_g), indicating high chain mobility, which rendered PU0 soft

and ductile, but concomitantly imparted poor water resistance. After the introduction of 5% APTMS, the PU5 film exhibited an increased number of crosslinking sites and hard phase regions, which led to a higher T_g, substantially enhanced mechanical properties (accompanied by reduced elongation at break), and markedly improved water resistance. The subsequent incorporation of Ca^{2+}-mediated ionic crosslinking further augmented the mechanical strength of PU5, albeit with a slight compromise in its water resistance. Collectively, the synergistic application of covalent self-crosslinking and ionic crosslinking strategies resulted in significant and comprehensive improvements in the performance of PU films.

Structural Characterization and Phase-separation Structure

FTIR, SEM-EDS, and XPS analyses were performed to further elucidate the chemical structure. As showed in Fig. S7 (in ESI), the FTIR spectrum of PEBA exhibits a characteristic peak at 3513 cm^{-1} ascribed to O—H stretching vibration, which is absent in the PU films.[37] Compared with the spectrum of PEBA, new characteristic bands appeared in the FTIR spectra of PU films at 1525 and 3362 cm^{-1}, corresponding to the bending and stretching vibrations of N—H bonds within urethane groups, respectively.[38,39] Notably, the C=O stretching band at 1727 cm^{-1} is broader in the PU films than in PEBA, reflecting the formation of additional C=O species originating from the urethane and carboxyl groups.[3,40] In addition, new bands at 1640 cm^{-1} observed in both PU and CPU films were assigned to the stretching vibration of hydrogen-bonded C=O in urea groups, proving the reaction between the amino groups of APTMS and —NCO groups of IPDI.[41] The intensities of these peaks increased with increasing APTMS content (Fig. S7 in ESI). These results demonstrate the successful synthesis of the designed self-crosslinked polyurethane. The surface morphology and elemental composition were further characterized by SEM-EDS (Figs. S8 and S9 in ESI). The surfaces of the CPU films were homogeneous and flat, with carbon, oxygen, calcium, nitrogen, and silicon uniformly distributed across the analyzed area (Fig. S8 in ESI). Compared to CPU0, the EDS spectrum of CPU5 reveals a new characteristic Si peak at 1.75 keV (Fig. S9a in ESI).[14] The XPS analysis of PU0 clearly displays O 1s, C 1s, N 1s, and Si 2p signals,[42,43] whereas the spectrum of CPU5 additionally exhibits a Ca 2p signal (Fig. S9b in ESI), confirming the successful incorporation of ionic crosslinking.

Based on the molecular structure design strategy employed in this work, the resulting CPU films are expected to feature a combination of diverse hydrogen bonds, Si—O—Si covalent cross-linking, and Ca–$(COO)_2$ structure (Fig. 2). XPS, XRD, and Raman mapping were performed to further investigate the microstructures of the PU films. The characteristic Si 2p peak was deconvoluted into two components: the Si $2p_{1/2}$ orbit (102.2 eV) and Si $2p_{3/2}$ orbit (101.8 eV (Fig. 2a)). The latter corresponds to Si(—O)$_3$ (Si—O—Si and Si—OH). The Ca 2p XPS spectrum exhibited two distinct peaks at 350.9 ($2p_{1/2}$) and 347.4 eV ($2p_{3/2}$) (Fig. 2b).

Notably, while the Ca $2p_{3/2}$ binding energy of $CaCl_2$ is reported at 348.0 eV,[44] the corresponding peak in the CPU5 film appears at 347.4 eV, which is characteristic of the Ca—$(COO)_2$ coordination structure, thereby confirming the successful formation of ionic crosslinking. Collectively, these results demonstrate that both Si—O—Si covalent crosslinking and Ca^{2+}-mediated ionic crosslinking are effectively established within CPU films. The XRD patterns of CPU0-CPU5 exhibit typical amorphous features, with a broad diffraction peak centered at approximately 20°, attributed to the aggregation of H-bonds (hard phase region) within the amorphous PU films (Fig. 2c).[41] As the degree of Si—O—Si covalent crosslinking increases, the intensity of this peak progressively increases, indicating an improvement in the hard-phase regions.

Raman spectroscopy was employed to resolve the distinct chemical domains within PU and CPU films.[45,46] Figs. 2(d)–2(e) show that the characteristic spectral region from 3400 cm^{-1} to 2850 cm^{-1} can be segmented into two distinct chemical environments, represented by the blue and red spectra corresponding to the blue and red regions, respectively. In the blue spectra, both the N—H and CH_2/CH_3 stretching vibrations exhibited relatively high intensities, indicating N—H-rich regions. In contrast, the red spectra display weaker N—H stretching signals along with stronger CH_2/CH_3 stretching vibrations, which are characteristic of N—H-poor regions associated with the soft segments. It has been reported that almost all N—H groups in solid-state PU films can form H-bonds at room temperature.[47] The typical domain size of the microphase-separated morphology in PU is smaller than the spatial resolution (200 nm step size) of the Raman images. Therefore, the N—H-rich regions could be identified as hard-phase-rich regions. Raman mapping revealed that these hard-phase-rich regions (blue regions) were uniformly dispersed throughout the soft domains (red regions) across the analyzed area, demonstrating a macroscopically homogeneous, yet microscopically phase-separated structure within the PU films. Multivariate curve resolution (MCR) was further applied to quantify the area fraction of the hard-phase-rich region through the full soft domains (Figs. 2d–2f and Fig. S10 in ESI). The proportion of hard phase-rich regions increased from 14.8% in PU0 to 25.8% in PU5, providing additional evidence for the formation of supplementary hydrogen bonds. Notably, no significant change in the hard-phase-rich region (about 25.7%) was observed after Ca^{2+} crosslinking. Based on the foregoing structural analysis, a schematic illustration of the microstructure of CPU films is presented in Fig. 2(g).

Dynamic Mechanical Analysis and Thermal Performance

The dynamic mechanical properties of PU films provide insight into the temperature dependence of the storage modulus and loss factor (tanδ). At temperatures below –20 °C, the macromolecular chains are frozen, and all films exhibit high storage moduli along with a low tanδ (Figs. 3a, 3b, and Fig. S11 in ESI). As the temperature increased, the storage moduli of all PU films declined rapidly owing to the enhanced chain segment mobility. At 25 °C, the storage moduli of PU5 and CPU5 reach 15.4 and 16.9 MPa, respectively, substantially higher than those of PU0 and CPU0 (7.0 and 7.8 MPa), indicating that the Si—O—Si crosslinking network restricts chain mobility and enhance film stiffness. All PU films exhibited a distinct broad peak in the tanδ curves, corresponding to the glass transition temperature (T_g) of the hard phase region.[48] In fact, the PU films exhibited a weak

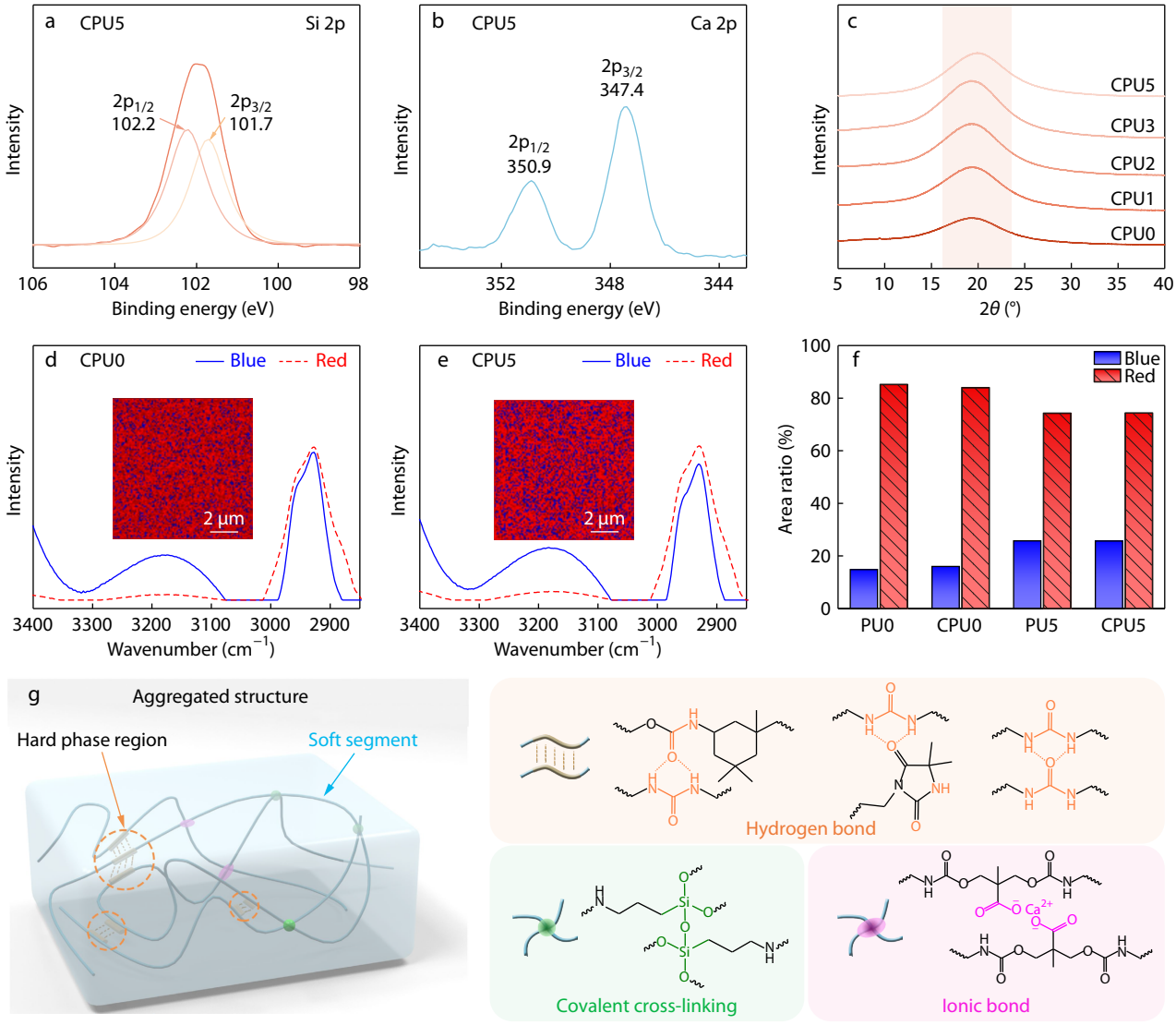

Fig. 2 Investigating the crosslinking mechanisms and micro-phase structure of CPU films. (a) Si 2p and (b) Ca 2p peaks in the CPU5 film; (c) XRD patterns of CPU films; Raman spectra of the N—H poor (red) and N—H rich regions (blue) within the (d) CPU0 and (e) CPU5. The insets are the reconstructed Raman image of the red and blue domains within the PU films obtained from the $-CH_2/CH_3$ and —NH stretching mode intensities (2850–3400 cm^{-1}). (f) The area ratio of red and blue domains with PU films from 2D Raman mapping; (g) The micro-phase structure of CPU film and several macromolecular interactions may exist in CPUs.

shoulder peak between –20 and 0 °C, which is consistent with the T_g of the PEBA soft segments.[49] This result is consistent with the Raman mapping findings, indicating the presence of a phase-separated structure within the PU film. Fig. 3(b) shows that PU0 and CPU0 display a T_g of approximately 13.9 °C, whereas the incorporation of APTMS shifts the T_g of PU5 to a higher temperature (30.5 °C). This increase in T_g is attributed to the combined effects of the Si—O—Si crosslinking network and formation of additional H-bonds. In addition, the tanδ curves of PU0 and CPU0 show broad peaks from –20 °C to 40 °C, followed by a sharp rise, indicative of chain slippage. However, the PU5 and CPU5 films exhibited broader tanδ peaks from –20 °C to 100 °C, probably due to the presence of the Si—O—Si crosslinking network, which effectively suppressed interchain slippage.

The thermal degradation behavior of the PU films at different temperatures was investigated under N_2 conditions (Figs. 3c and 3d). All the films displayed similar thermal degradation profiles, but the residual char content increased for PU5 and CPU5. Thermal degradation in polyurethane materials is typically initiated at weak linkages, such as urethane and urea groups, owing to their relatively low bond energies. The initial degradation temperature ($T_{10\%}$), defined as the temperature corresponding to 10% weight loss, serves as a key indicator of thermal stability. As summarized in Table S3 (in ESI), the $T_{10\%}$ of the PU0 film was 279 °C. However, the slight decrease in $T_{10\%}$ observed for PU5 and CPU5 could be attributed to the increased content of urethane and urea bonds resulting from the incorporation of 5% APTMS. These bonds represent the weakest point within polyurethane materials, and thus significantly influence the initial degradation temperature.[47,50] In contrast, the formation of the Si—O—Si crosslinking network primarily improved the thermal-oxidative stability at elevat-

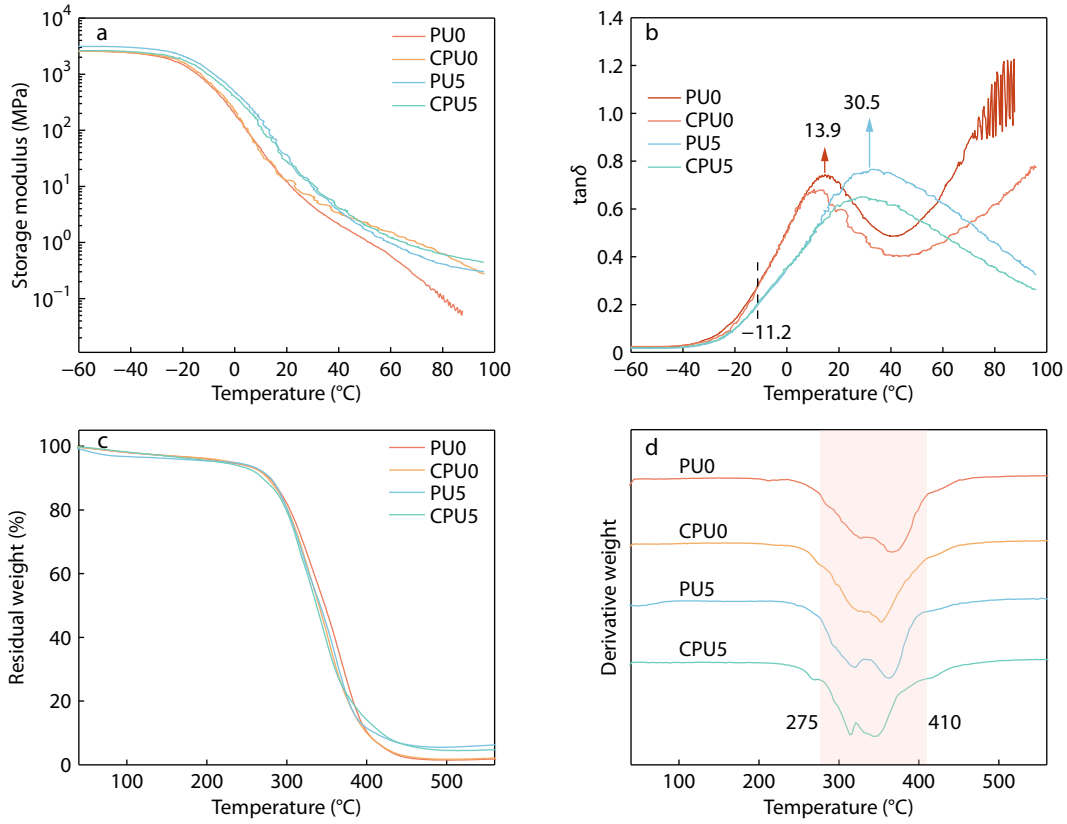

Fig. 3 Thermal property of PU films. (a) Storage modulus and (b) tanδ of PU films from –60 °C to 100 °C; (c) TG and (d) DTG thermograms of PU films from 40 °C to 560 °C.

ed temperatures ($T_{90\%}$), as evidenced by the higher residual mass of CPU5 at 600 °C.[51,52] The primary degradation process of PU films, corresponding to a weight loss from 10% to 90%, occurs predominantly between 275 and 410 °C. During this stage, the ester groups on the soft segments decomposed to form oligomers or monomers.[47] With a further temperature increase, the oligomers or monomers undergo subsequent thermal decomposition, leading to a rapid loss of the sample mass.

Mechanical Property and Fatigue Resistance

To evaluate the mechanical properties of the PU films, tensile stress-strain tests were conducted (Fig. 4, Fig. S12 and Table S4 in ESI). As shown in Fig. S12 (in ESI), pure PU0 exhibited the lowest tensile strength (0.20 MPa), toughness (2.90 MJ/m^3), and high elongation at break (3023%). The low tensile strength of PU0 is primarily attributed to its linear, non-crosslinked structure. This explanation is further supported by our DMA results, which show a relatively low T_g (about 13.9 °C) for PU0, confirming the high mobility and easy slippage of the polymer chains under stress. After the introduction of APTMS, the enhanced Si—O—Si crosslinking density and more abundant H-bonds within the film resulted in a higher T_g (as indicated by the DMA result) and more hard-phase-rich regions (from the Raman results). The Si—O—Si crosslinking network and hard-phase-rich regions hinder molecular chain mobility and effectively dissipate energy, thereby significantly improving the tensile strength, Young's modulus and toughness, to 10.1 MPa, 3.94 MPa and 34.6 MJ/m^3 for PU5, respectively, which are 50.5, 3.7 and 11.9 times higher than those of the PU0 film (Figs. 4a–4c and Fig. S12 in ESI). However, the Si—O—Si crosslinking network hindered the molecular chain mobility, which significantly reduced the elongation at break (858%).

The introduction of Ca—$(COO)_2$ coordination structures further enhanced the tensile strength of the PU films. The tensile strength of the PU5 films increased and then decreased slightly as the concentration of $CaCl_2$ solution increased from 1 wt% to 7 wt% (Fig. S13 in ESI), and 5 wt% $CaCl_2$ solution was selected as the coagulation bath. Following Ca^{2+} crosslinking, both the tensile strength and modulus increased markedly across all PU films (Fig. S14 in ESI). Specifically, the CPU5 film achieve a tensile strength of 12.7 MPa, a modulus of 6.24 MPa, and a toughness of 43.0 MJ/m^3, corresponding to enhancements of 1.25-, 1.58-, and 1.24-fold relative to the single covalent crosslinked PU film (PU5), respectively. Compared with a single Ca^{2+} ionic crosslinked PU film (CPU0), the mechanical properties of the CPU5 film were dramatically improved (35.3-, 4.52-, and 6.76-fold, respectively). These results clearly demonstrate that the combination of covalent self-crosslinking and ionic crosslinking exhibits a strong synergistic effect, wherein the covalent network provides a permanent structural scaffold, while the ionic crosslinks act as reversible energy-dissipating units, collectively leading to a remarkable enhancement in overall mechanical performance. The excellent mechanical performance of CPU5 was further evidenced by photographs of its tensile behavior (Figs. 4d and 4e). The

https://doi.org/10.1007/s10118-026-3773-8

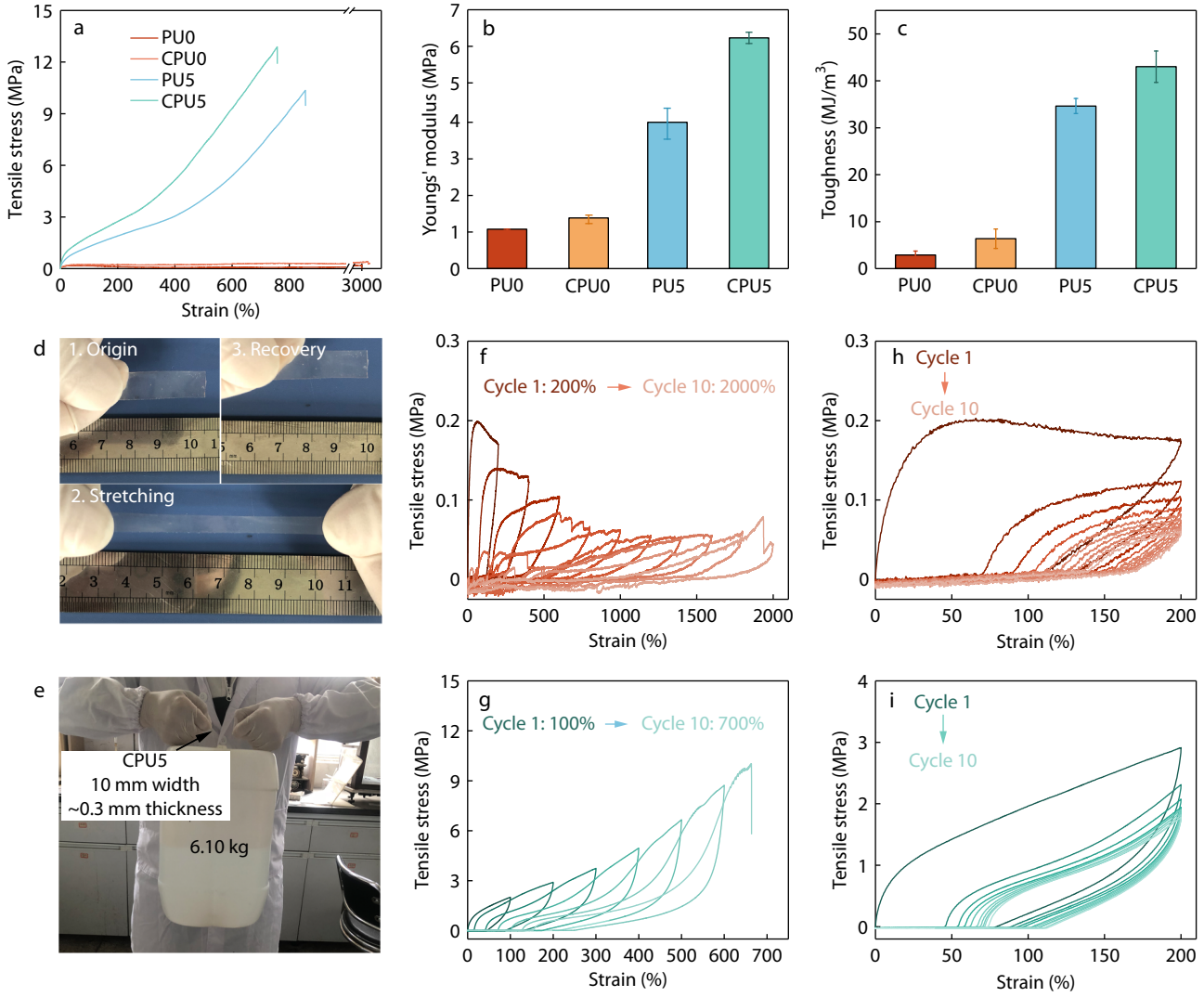

Fig. 4 Mechanical properties and fatigue resistance. (a) The tensile strength of PU films; The summary of (b) Young's modulus and (c) toughness of PU films. (d, e) Photos showing tensile behaviors of the CPU5 film. Cyclic tensile test curves of (f) film PU0 and (g) CPU5 in successive loading-unloading cycles with increasing strains but no resting time. Cyclic tensile test curves of (h) film PU0 and (i) CPU5 in successive loading-unloading cycles with 200% strains but no resting time.

CPU5 film can be stretched to approximately seven times its original length and can lift a 6 kg bottle of water.

To gain a deeper insight into the strengthening and toughening mechanisms, the fatigue resistances of the CPU5 and PU0 films were systematically evaluated (Figs. 4f–4i, Figs. S15 and S16 in ESI). Cyclic tensile tests were conducted with progressively increasing strains. The results show that the area of the hysteresis loop increases with the applied strain, indicating a positive correlation between the energy dissipation efficiency and strain level (Fig. 4f and Fig. S15 in ESI). For the PU0 film, as the strain increases from 200% to 2000%, the hysteresis loop area ranges from 0.30 MJ/m^3 to 0.37 MJ/m^3, accompanied by a gradual decrease in tensile strength (Fig. S15a in ESI). This behavior may originate from the dissociation of weak H-bond domains under tension. In contrast, the CPU5 film exhibits a substantial increase in hysteresis energy from 1.0 MJ/m^3 to 15.1 MJ/m^3 and an increase in tensile strength from 2.0 MPa to 10.0 MPa (Fig. S15c in ESI). This enhancement can be rationalized by a gradient dissociation mechanism, wherein weak hydrogen bonds preferentially rupture at low strains to dissipate energy, whereas high strains progressively engage the strong hard-phase regions and ionic crosslinks in the energy dissipation process.[5,53]

Subsequently, the PU0 and CPU5 films were subjected to ten consecutive tensile loading-unloading cycles at a fixed strain of 200% without resting intervals (Figs. 4h and 4i). The PU0 film shows pronounced hysteresis in the first cycle, which is attributed to the irreversible fracture of weak hydrogen-bonded domains (Fig. 4h and Figs. S15b–S15d in ESI). However, CPU5 exhibits relatively low hysteresis during cyclic stretching, which is attributed to its hard domains and flexible cooperative network design. The recovery behavior of the hysteresis strain in CPU5 was further investigated through cyclic tensile tests with resting times of 5 min and 2 h (Fig. S16 in ESI). After a 5 min rest, the recovery ratio of the hysteresis strain reached 71%, suggesting the rapid recovery of

https://doi.org/10.1007/s10118-026-3773-8

most of the residual strain. Notably, the stretched CPU5 film completely recovered its initial state after 2 h of rest.

In summary, these results demonstrate that the CPU5 film combines favorable mechanical properties with excellent recovery of the hysteresis strain. Based on the aforementioned structural and mechanical analyses, we propose the following strengthening and toughening mechanisms: First, multiple H-bonds within the hard-phase regions act as sacrificial bonds, dissipating a portion of the mechanical energy.[41] Second, the Ca—$(COO)_2$ ionic crosslinking structure contributes to the enhanced hardness and strength of the CPU5 film.[6] Meanwhile, the strong covalent Si—O—Si crosslinks between molecular chains preserve the network integrity under large deformations, thereby significantly improving the tensile strength and toughness.[54] Additionally, the abundant H-bonds within the hard-phase regions may form a physical crosslinking network and restrict the mobility of chain segments. The flexible chain segments impart conformational adaptability, dynamically reorganizing under stress to mitigate localized stress concentrations and thus potentially reduce permanent deformation.

Adhesion Property

Solvent-free adhesives have attracted considerable attention owing to the elimination of volatile organic compound (VOC) emissions. Notably, the PU5 film exhibits a broad glass transition range spanning from –20 °C to 100 °C with a peak value at approximately 30.5 °C. Because of their abundant hydrogen bonds and wide glass transition range, the PU5 films have been explored as solvent-free adhesives. Single-lap joint samples were fabricated *via* a simple two-step process involving heating, followed by cooling (Fig. 5a). Upon heating, the softening of the PU5 film and the dissociation of dynamic H-bonds provided sufficient chain mobility to establish intimate contact between the PU film and the substrates. Upon cooling, the re-association of H-bonds or potential formation of covalent bonds between the polymer chains and substrates contributes to a comparatively high adhesive strength.[55]

The lap shear strengths of the samples were investigated to evaluate the adhesion performance of the PU5 adhesive. As shown in Figs. 5(b) and 5(d), the lap shear strength on the glass substrates was tested at different temperatures (50–90 °C). The PU5 film exhibited an increasing lap shear strength on glass substrates as the bonding temperature rose from 50 °C (1.63 MPa, Glass-50) to 70 °C (2.69 MPa, Glass-70). At relatively low temperatures, the adhesion strength of the PU film was primarily mediated by H-bonds between the PU5 film and the substrates.[56] Increasing the temperature enhances the mobility of the molecular segments, promoting better contact between the molecular chains and glass surface. Concurrently, the increase in temperature facilitated the formation of partial Si—O—Si or Si—O—M covalent bonds on the substrate surfaces, contributing to the observed improvement in lap shear strength.[57] According to Wang *et al.*, the degree of H-bond association in PU adhesives decays gradually above 80 °C.[58] Therefore, although a further temperature increase may enhance covalent interactions, it also leads to significant dissociation of H-bonds, thereby limiting further gains in lap shear strength. Additionally, the PU5 adhesive exhibited a moderate adhesion strength of 1.50 MPa

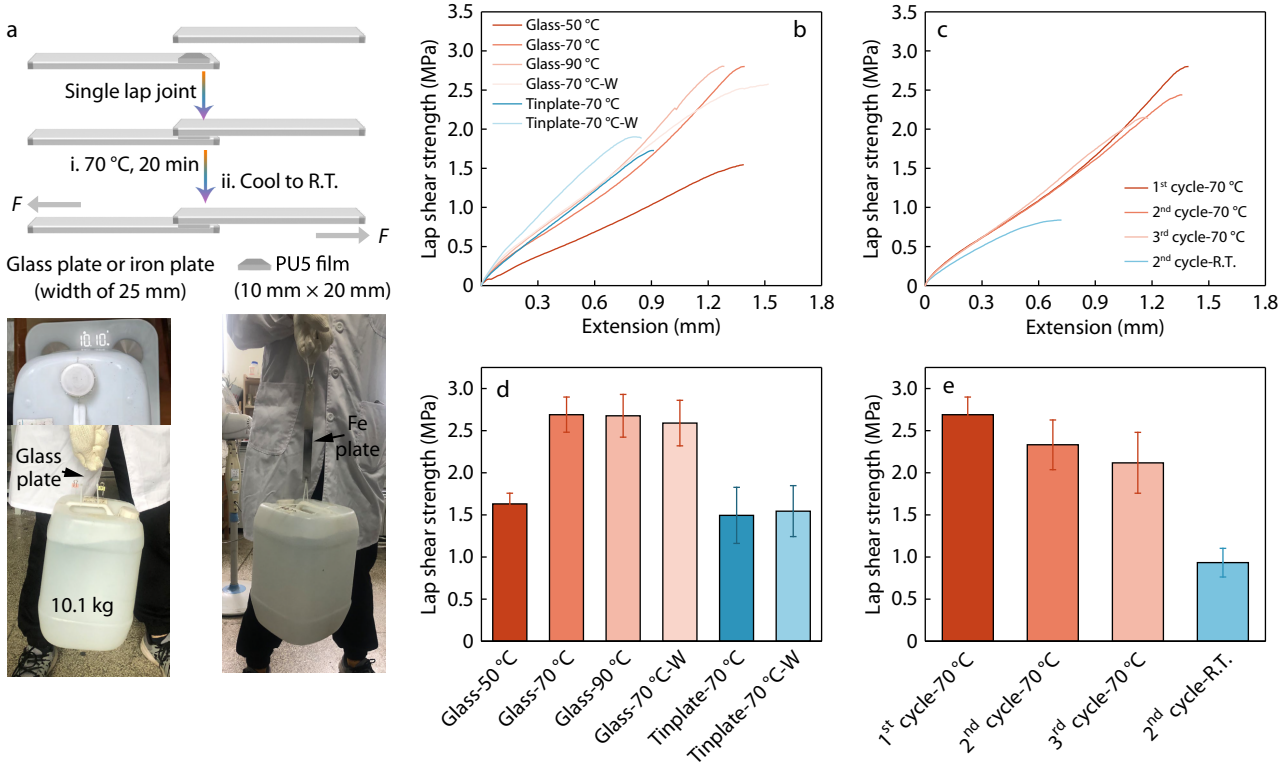

Fig. 5 Adhesive properties of the PU5 film. (a) The process of PU5 adhesive in bonding glass or tinplate sheets; (b) Lap-shear strength-extension curves and (d) lap-shear strength of the PU5 film in gluing glass and tinplate under different condition; (c) Lap strength–extension curves and (e) lap-shear strength of the PU5 film in gluing glass with different recycles.

https://doi.org/10.1007/s10118-026-3773-8

when bonding tinplates at a heating temperature of 70 °C (Tinplate-70). Furthermore, the adhered glass and tinplate joints were immersed in water for 1 h prior to lap shear testing to investigate the influence of moisture on the bonding performance. The bonding strengths of glass (Glass-70-W) and tinplate (Tinplate-70-W) were 2.60 and 1.54 MPa, respectively, indicating that the PU5 adhesive exhibited minimal sensitivity to water. This result is consistent with the low water absorption of the PU5 film. According to the water resistance results of the PU films, the water absorption of the PU5 film significantly decreased to 5.5% after immersion in water for 24 h, compared with 19.9% for PU0 (Fig. S17 in ESI). This demonstrates the effectiveness of the covalent crosslinking strategy in enhancing the water resistance. In addition, the adhered glass (Glass-70) and tinplate (Tinplate-70) joints were able to lift bottled water weighing 10 kg, further confirming the high lap shear strength (Fig. 5a).

More importantly, the PU5 adhesive exhibited excellent recyclability and recoverability in bonding glass substrates (Figs. 5c and 5e). After lap-shear testing to failure, the separated glass pieces were recontacted, gently pressed, and heated at 70 °C for 20 min to achieve rebonding. The adhesion strengths of re-bonded glass joints in the 2nd and 3rd cycles reached 2.33 and 2.12 MPa, respectively. To elucidate the origin of the slight decrease in the rebonding strength of PU5 after adhesion cycles, we performed control experiments using PU0 (without APTMS). As shown in Fig. S18 (in ESI), the lap shear strength of PU0 remained virtually unchanged over three consecutive bonding and rebonding cycles at 70 °C. This observation indicates that the slight loss in the bonding strength of PU5 might be attributable to the irreversible breakage of covalent bonds (Si—O—Si) formed between the adhesive and the glass surface. Notably, even without heating, the re-bonded joint (2nd cycle-R.T.) exhibited an adhesion strength of 0.93 MPa, assigned to the rapid reformation of H-bonds at the interface. Upon heating to 70 °C, the dissociation of H-bonds imparts sufficient chain mobility, enabling intimate contact between the adhesive and the substrate, which facilitates the re-construction of H-bonds, yielding a high re-bonding strength. Overall, the PU5 adhesive demonstrated high adhesion strength across various substrates and retained its bonding performance under humid conditions, making it a promising candidate for a wide range of practical applications.

Antibacterial Efficacy and Cell Compatibility

The surfaces of conventional polymers are prone to microbial contamination. The accumulation of microorganisms on the surface of materials has adverse effects on human life, such as mildew, release of unpleasant odors, cross-contamination, and cross-infection.[27] It has been reported that HD undergoes a chlorination process, and the N—H bonds on the hydantoin ring can be converted to N—Cl bonds, thereby imparting significant antimicrobial properties to the material.[26] After chlorination, the Cl in the CPU5-Cl film was detected by EDS, and the active chlorine content was determined *via* titration, yielding a result of 0.26% (Figs. S18 and S19 in ESI). Herein, the antibacterial behaviors of the PU films were evaluated against Gram-positive *S. aureus* (6.15×10^6 CFU/sample) and Gram-negative *E. coli* (1.57×10^7 CFU/sample). As illustrated in Figs. 6(a)–6(f) and Fig. S20 in ESI, only a slight reduction in bacterial viability was observed after 60 min of contact with PU0, CPU0, PU5, and CPU5 films. In contrast, the CPU5-Cl film exhibited a high antibacterial efficiency, with bacterial survival rates decreasing substantially with increasing contact time (Figs. 6e, 6f, and Fig. S20 in ESI). After 5 min of contact, approximately 20.2% of *S. aureus* and 23.0% of *E. coli* were inactivated. After 60 min, virtually no *S. aureus* colonies and only a few scattered *E. coli* colonies were observed on the agar plates, corresponding to antibacterial efficiencies of 97.8% against *S. aureus* and 92.4% against *E. coli*. The substantial enhancement of antibacterial activity following chlorination underscores the critical role of oxidative halogen (Cl^+) species in bacterial inactivation.

N-Halamine compounds exert antibacterial effects by transferring Cl^+ to biological receptors upon contact with bacterial cells. This process leads to the oxidation of thiol groups or the halogenation of amino groups in essential proteins, thereby inactivating bacteria.[26] However, Cl^+ exhibits relatively poor stability when exposed to sunlight or ultraviolet radiation. Accordingly, the storage stability and recoverability of antibacterial function were evaluated (Fig. S19 in ESI). After 45 days of storage in the dark, the Cl^+ content of CPU5-Cl decreased to approximately 0.13%, corresponding to 50% of its original value. Importantly, the lost chlorine could be restored through rechlorination, enabling the CPU5 film to maintain long-lasting and highly effective antimicrobial performance.

Given that the chlorination process may potentially compromise material properties,[59] we systematically evaluated the impact of the chlorination process on other properties (*e.g.*, biocompatibility, mechanical properties, and thermal properties) of CPU films. As presented in Figs. 6(g), 6(h) and Fig. S21 (in ESI), the cell biocompatibility of the CPU5-Cl film (cell viability about 83.5%) was comparable to that of CPU5 (about 86.3%). Fluorescence images revealed negligible red fluorescence from dead cells after 24 h of co-culture, demonstrating that the CPU5-Cl film had no obvious toxicity. This phenomenon might result from the contact-killing mechanism of HD on bacterial receptors rather than a substantial release of free chlorine.[20] Furthermore, the chlorination process had virtually no effect on the microphase structure (from 3D Raman, Fig. S22 in ESI), revealing that chlorination primarily occurred on the film surface. Consequently, the mechanical properties (tensile strength, elongation, modulus, and toughness) and T_g of CPU5-Cl were comparable to those of the CPU5 film (Figs. S23 and S24 in ESI). Additionally, the conversion of N—H to N—Cl on the film surface contributed to improved water resistance (Fig. S17 in ESI). Collectively, these results demonstrate that the chlorination process causes negligible damage to the structural integrity, mechanical performance, and thermal properties of PU films, while effectively enhancing their antibacterial activity and water resistance (Fig. 6i).

As shown in Table S5 (in ESI), we compared the CPU film with representative WPUs from the recent literature. While the tensile strength of CPU5 is lower than that of some robust WPUs (40–60 MPa), it is comparable to or better than that of bio-based WPUs and silane-crosslinked WPUs. Although robust WPUs have achieved higher strengths, such systems typically require complex molecular design. In terms

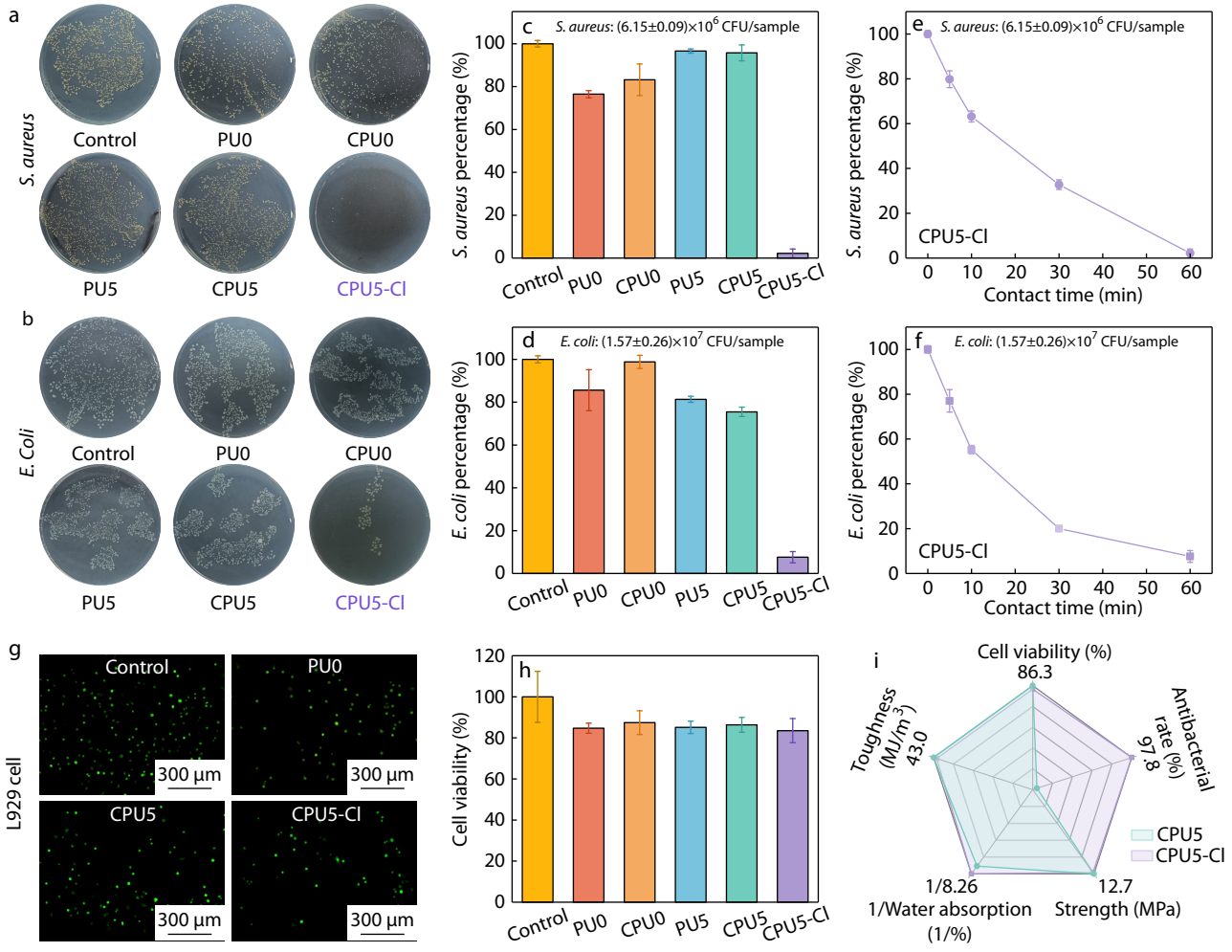

Fig. 6 Antibacterial efficacy and cell compatibility of PU films. Photos of antibacterial behaviors of PU films against (a) *S. aureus* and (b) *E. coli*; Antibacterial properties of PU films with 60 min incubation at 37 °C against (c) *S. aureus* and (d) *E. coli*; Antibacterial properties of CPU5-Cl film with 5–60 min incubation at 37 °C against (e) *S. aureus* and (f) *E. coli*; (g) Live/dead staining results and (h) cell viability of L929 cells after co-culture with PU films; (i) Radar plots comparing physicochemical properties and bioactivities before and after chlorination process.

of water resistance, CPU5 shows wet-state stability comparable to that of WPUs owing to its covalent crosslinking network. Regarding antibacterial activity, unlike most reported WPUs that rely on leachable agents (*e.g.*, Zn, Cu, and AgNPs), this CPU5 employs a non-leaching N-halamine contact-killing mechanism, avoiding environmental toxicity concerns. Critically, while most studies have focused on optimizing a single property (*e.g.*, mechanical strength, water resistance, or antibacterial activity), the CPU5 films simultaneously achieve high strength, toughness, excellent water resistance, satisfactory antibacterial activity, good cytocompatibility, and recoverable adhesion. This balanced multifunctionality exhibits a distinctive advantage and addresses the growing demand for multifunctional materials for biomedical applications.

CONCLUSIONS

Self-crosslinking combined with an ionic crosslinking strategy was successfully developed to fabricate high-performance PU films. The construction of microphase-separated structures (with a hard phase region accounting for 25.7%) and the introduction of Si—O—Si covalent crosslinking imparted excellent water resistance (water absorption: 5.5%) and superior mechanical properties (tensile strength: 10.1 MPa, Young's modulus: 3.94 MPa). The subsequent incorporation of Ca^{2+} ionic crosslinking further promoted the mechanical properties (tensile strength: 12.7 MPa, Young's modulus: 6.24 MPa). The abundant H-bonds within the hard phase regions enable efficient energy dissipation through reversible dissociation and recombination, endowing the PU film with exceptional toughness (43.0 MJ/m^3) and recoverability. Notably, the PU5 film functioned as a solvent-free adhesive, achieving high adhesion strengths of 2.69 MPa on glass and 1.5 MPa on tinplate. More importantly, the PU5 adhesive exhibited reusability and retained its adhesive performance under humid conditions. Upon chlorination, the resulting CPU5-Cl film exhibited potent antibacterial activity (97.8% against *S. aureus* and 92.4% against *E. coli*), along with outstanding biocompatibility. Therefore, these combined attributes render the developed PU films highly promising for a broad range of applications, including bioadhesives, biomedical scaffolds, and electronic devices.

https://doi.org/10.1007/s10118-026-3773-8

Conflict of Interests

The authors declare no interest conflict.

Electronic Supplementary Information

Electronic supplementary information (ESI) is available free of charge in the online version of this article at http://doi.org/10.1007/s10118-026-3773-8.

Data Availability Statement

The data that support the findings of this study are available from the corresponding author upon reasonable request.

ACKNOWLEDGMENTS

This work was financially supported by the Natural Science Foundation of Jiangxi Province (Nos. 20242BAB21024 and 20242BAB20181), the National Natural Science Foundation of China (No. 52303120), and the Science-Technology Foundation for Young Scientists of Jiangxi Province (No. 20244BCE52214).

REFERENCES

1 Zhang, Y.; Lin, R.; Li, H.; Shi, Y.; Liu, Y.; Zhou, C. Investigation of the migration ability of silicone and properties of waterborne polyurethanes. *Int. J. Adhes. Adhes.* **2020**, *102*, 102654.
2 Li, X.; Xie, Y.; Huang, M.; Umeyama, T.; Ohara, T.; Imahori, H. Effective role of eco-friendly acetyl tributyl citrate in large-scale catalyst-free synthesis of waterborne polyurethanes without volatile organic compounds. *J. Clean. Prod.* **2019**, *237*, 117543.
3 Pei, A.; Malho, J.-M.; Ruokolainen, J.; Zhou, Q.; Berglund, L. A. Strong nanocomposite reinforcement effects in polyurethane elastomer with low volume fraction of cellulose nanocrystals. *Macromolecules* **2011**, *44*, 4422−4427.
4 Li, Z.; Zhu, Y. L.; Niu, W.; Yang, X.; Jiang, Z.; Lu, Z. Y.; Liu, X.; Sun, J. Healable and recyclable elastomers with record-high mechanical robustness, unprecedented crack tolerance, and superhigh elastic restorability. *Adv. Mater.* **2021**, e2101498.
5 Xu, F.; Li, H.; Li, Y. Sea cucumber-inspired polyurethane demonstrating record-breaking mechanical properties in room-temperature self-healing ionogels. *Adv. Mater.* **2024**, *36*, 2412317.
6 Huang, Y.; Yu, H.; Xiao, C. Effects of Ca^{2+} crosslinking on structure

Graphical Abstract

Self-crosslinking Waterborne Polyurethane with Antibacterial Performance and Solvent-free Adhesiveness

Shan-Shan Li, Sang-Qi Chen, Yi Xiao, Wen-Jie Xu, and Xing-Huan Lin

Gannan Normal University

A strategy combining self-crosslinking and ionic crosslinking is used to fabricate waterborne polyurethane with a microphase separated structure. This strategy dramatically enhances the mechanical strength and water resistance. Waterborne polyurethane can serve as a recoverable solvent-free adhesive. Moreover, this film exhibits high antibacterial efficiency and satisfactory cytocompatibility for biomedical applications.

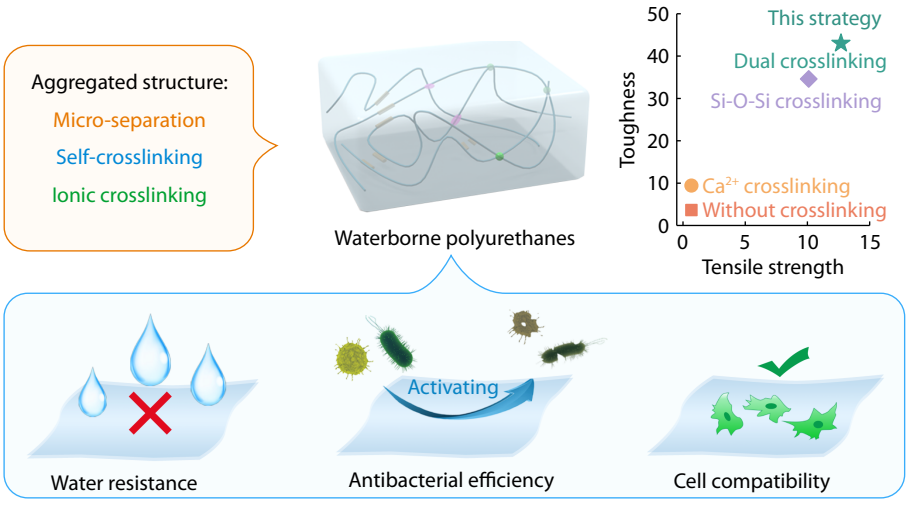

Chinese J. Polym. Sci. 2026 *https://doi.org/10.1007/s10118-026-3773-8*

and properties of waterborne polyurethane-carboxymethylated guar gum films. *Carbohydr. Polym.* **2006**, *66*, 500–513.
7 Zeng, W.; Jin, Y.; Zhou, R.; Li, Y.; Chen, H. Double crosslinked networks waterborne polyurethane with self-healing, recyclable and antibacterial functions based on dynamic bonds and used for temperature/light sensor. *Chem. Eng. J.* **2024**, *482*, 148994.
8 Wang, X.; Zhan, S.; Lu, Z.; Li, J.; Yang, X.; Qiao, Y.; Men, Y.; Sun, J. Healable, recyclable, and mechanically tough polyurethane elastomers with exceptional damage tolerance. *Adv. Mater.* **2020**, *32*, e2005759.
9 Wang, F.; Yang, Z.; Li, J.; Zhang, C.; Sun, P. Bioinspired polyurethane using multifunctional block modules with synergistic dynamic bonds. *ACS Macro Lett.* **2021**, *10*, 510–517.
10 Tan, M. W. M.; Thangavel, G.; Lee, P. S. Rugged soft robots using tough, stretchable, and self-healable adhesive elastomers. *Adv. Funct. Mater.* **2021**, *31*, 2103097.
11 Yao, Y.; Liu, B.; Xu, Z.; Yang, J.; Liu, W. An unparalleled h-bonding and ion-bonding crosslinked waterborne polyurethane with super toughness and unprecedented fracture energy. *Mater. Horiz.* **2021**, *8*, 2742–2749.
12 Zheng, B.; Liu, T.; Liu, J.; Cui, Y.; Ou, R.; Guo, C.; Liu, Z.; Wang, Q. Spider silk-inspired dynamic covalent polyurethane with fast repairing, shape memory, and strong dynamic adhesion *via* lignin enhanced microphase separation. *Compos. Part B-Eng.* **2023**, *257*, 110697.
13 Ying, W. B.; Yu, Z.; Kim, D. H.; Lee, K. J.; Hu, H.; Liu, Y.; Kong, Z.; Wang, K.; Shang, J.; Zhang, R.; Zhu, J.; Li, R. W. Waterproof, highly tough, and fast self-healing polyurethane for durable electronic skin. *ACS Appl. Mater. Interfaces* **2020**, *12*, 11072–11083.
14 Li, S.; Lin, X.; Liu, Y.; Li, R.; Ren, X.; Huang, T.-S. Phosphorus-nitrogen-silicon-based assembly multilayer coating for the preparation of flame retardant and antimicrobial cotton fabric. *Cellulose* **2019**, *26*, 4213–4223.
15 Chen, J.; Zhu, C.; Deng, H.; Qin, Z.; Bai, Y. Preparation and characterization of the waterborne polyurethane modified with nanosilica. *J. Polym. Res.* **2008**, *16*, 375–380.
16 Zhu, Z.; Zhao, Y.; Zhang, Y.; Zhang, S.; Li, W.; Ye, G.; Ma, X.; Zhang, X.; Bi, H. Self-healing, highly stretchable, and 3D printable thiol-functionalized cellulose nanofibers/waterborne polyurethane composites for flexible electronic monitoring. *Chem. Eng. J.* **2025**, *506*, 159835.
17 Wang, Y.; Qiu, F.; Xu, B.; Xu, J.; Jiang, Y.; Yang, D.; Li, P. Preparation, mechanical properties and surface morphologies of waterborne fluorinated polyurethane-acrylate. *Prog. Org. Coat.* **2013**, *76*, 876–883.
18 Xiong, W.; Chen, B.; Peng, J.; Luo, X.; Pan, X.; Xiao, Z.; Gong, W.; Huang, Z.; Chu, Z.; Zhang, X.; Zhou, C.; Liu, Y. A dual-crosslinking strategy for waterborne polyurethane coatings to achieve outstanding anti-smudge and anti-corrosion properties. *Chem. Eng. J.* **2024**, *490*, 151509.
19 Lin, X.; Yin, M.; Liu, Y.; Li, L.; Ren, X.; Sun, Y.; Huang, T.-S. Biodegradable polyhydroxybutyrate/poly-ε-caprolactone fibrous membranes modified by silica composite hydrol for super hydrophobic and outstanding antibacterial application. *J. Ind. Eng. Chem.* **2018**, *63*, 303–311.
20 Artus, G. R. J.; Jung, S.; Zimmermann, J.; Gautschi, H. P.; Marquardt, K.; Seeger, S. Silicone nanofilaments and their application as superhydrophobic coatings. *Adv. Mater.* **2006**, *18*, 2758–2762.
21 Zhang, Y.; He, X.; Ding, M.; He, W.; Li, J.; Li, J.; Tan, H. Antibacterial and biocompatible cross-linked waterborne polyurethanes containing gemini quaternary ammonium salts. *Biomacromolecules* **2018**, *19*, 279–287.
22 Wang, Y.; Chen, R.; Li, T.; Ma, P.; Zhang, H.; Du, M.; Chen, M.; Dong, W. Antimicrobial waterborne polyurethanes based on quaternary ammonium compounds. *Ind. Eng. Chem. Res.* **2019**, *59*, 458–463.
23 Wang, R.; Xiang, T.; Zhao, W. F.; Zhao, C. S. A facile approach toward multi-functional polyurethane/polyethersulfone composite membranes for versatile applications. *Mater. Sci. Eng. C Mater. Biol. Appl.* **2016**, *59*, 556–564.
24 Zhang, Y.; He, W.; Li, J.; Wang, K.; Li, J.; Tan, H.; Fu, Q. Gemini quaternary ammonium salt waterborne biodegradable polyurethanes with antibacterial and biocompatible properties. *Mater. Chem. Front.* **2017**, *1*, 361–368.
25 He, W.; Zhang, Y.; Li, J.; Gao, Y.; Luo, F.; Tan, H.; Wang, K.; Fu, Q. A novel surface structure consisting of contact-active antibacterial upper-layer and antifouling sub-layer derived from gemini quaternary ammonium salt polyurethanes. *Sci. Rep.* **2016**, *6*, 32140.
26 Dong, A.; Wang, Y. J.; Gao, Y.; Gao, T.; Gao, G. Chemical insights into antibacterial n-halamines. *Chem. Rev.* **2017**, *117*, 4806–4862.
27 Sun, X.; Cao, Z.; Porteous, N.; Sun, Y. An N-halamine-based rechargeable antimicrobial and biofilm controlling polyurethane. *Acta Biomater.* **2012**, *8*, 1498–1506.
28 Li, S.; Lin, X.; Gong, S. High strength and toughness transparent waterborne polyurethane with antibacterial performance. *Prog. Org. Coat.* **2022**, *172*, 107163.
29 Li, S.; Lin, X.; Gong, S. Waterborne polyurethane assembly multifunctional coating for hydrophobic and antibacterial fabrics. *Cellulose* **2022**, *29*, 7397–7411.
30 Baek, S. H.; Kim, J. H. Polyurethane composite foams including silicone-acrylic particles for enhanced sound absorption *via* increased damping and frictions of sound waves. *Compos. Sci. Technol.* **2020**, *198*, 108325.
31 Hwang, T.; Lee, H. J.; Hwang, S.; Yang, H.; Kim, H.; Jang, S.; Jeong, H. E.; Ryoo, Z. Y.; Yeo, J. Self-adhesive polyurethane *via* selective photo-polymerization for biocompatible epidermal soft sensor and thermal heater. *Appl. Mater. Today* **2022**, *27*, 101479.
32 Wang, D.; Li, J.; Wang, Y.; Olalekan Omoniyi, A.; Fu, Z.; Zhang, J.; Su, Z. Water-based polyurethane adhesive films with enhanced bonding strength capable of in situ and high-efficient deposition on metal surface. *Chem. Eng. J.* **2022**, *431*, 134055.
33 Wang, Y.; Yang, L.; Zhang, L.; Huang, H.; Qian, B.; Gu, S.; You, Z. Solvent-free synthesis of self-healable and recyclable crosslinked polyurethane based on dynamic oxime-urethane bonds. *Chinese J. Polym. Sci.* **2023**, *41*, 1725–1732.
34 Li, M.; Li, W.; Guan, Q.; Dai, X.; Lv, J.; Xia, Z.; Ong, W. J.; Saiz, E.; Hou, X. A tough reversible biomimetic transparent adhesive tape with pressure-sensitive and wet-cleaning properties. *ACS Nano* **2021**, *15*, 19194–19201.
35 Lin, X.; Zhang, H.; Li, S.; Huang, L.; Zhang, R.; Zhang, L.; Yu, A.; Duan, B. Polyphenol-driving assembly for constructing chitin-polyphenol-metal hydrogel as wound dressing. *Carbohydr. Polym.* **2022**, *290*, 119444.
36 Hu, N.; Rao, Y.; Sun, S.; Hou, L.; Wu, P.; Fan, S.; Ye, B. Structural evolution of silica gel and silsesquioxane using thermal curing. *Appl. Spectrosc.* **2016**, *70*, 1328–1338.
37 Deng, H.; Yu, Z.; Chen, S.; Fei, L.; Sha, Q.; Zhou, N.; Chen, Z.; Xu, C. Facile and eco-friendly fabrication of polysaccharides-based nanocomposite hydrogel for photothermal treatment of wound infection. *Carbohydr. Polym.* **2020**, *230*, 115565.
38 Hsieh, C. T.; Hsu, S. H. Double-network polyurethane-gelatin hydrogel with tunable modulus for high-resolution 3D bioprinting. *ACS Appl. Mater. Interfaces* **2019**, *11*, 32746–32757.
39 Lin, J.; Wang, L.; Liu, L.; Lu, K.; Li, G.; Yang, X. Two-stage interface enhancement of aramid fiber composites: Establishment of hierarchical interphase with waterborne polyurethane sizing and oxazolidone-containing epoxy matrix. *Compos. Sci. Technol.* **2020**, *193*, 108114.

40 Hung, K. C.; Hsu, S. H. Polymer surface interacts with calcium in aqueous media to induce stem cell assembly. *Adv. Healthc. Mater.* **2015**, *4*, 2186–2194.

41 Liang, H.; Lu, Q.; Liu, M.; Ou, R.; Wang, Q.; Quirino, R. L.; Luo, Y.; Zhang, C. UV absorption, anticorrosion, and long-term antibacterial performance of vegetable oil based cationic waterborne polyurethanes enabled by amino acids. *Chem. Eng. J.* **2020**, *421*, 127774.

42 Chen, S. F.; Su, J. L.; Zhang, S. X.; Hu, Z.; Bao, J. X.; Cha, X. Y.; Zhao, W. F.; Zhao, C. S. Bipolar and NIR-responsive polyurethane microspheres as a bifunctional adsorbent for simultaneous capture of bacteria and removal of dyes. *Chinese J. Polym. Sci.* **2026**, *44*, 315–330.

43 Fan, H.; Song, X.; Xu, Y.; Yu, J. Insights into the modification for improving the surface property of calcium sulfate whisker: Experimental and DFT simulation study. *Appl. Surf. Sci.* **2019**, *478*, 594–600.

44 Hu, X.; Kang, F.; Yang, B.; Zhang, W.; Qin, C.; Gao, Y. Extracellular polymeric substances acting as a permeable barrier hinder the lateral transfer of antibiotic resistance genes. *Front. Microbiol.* **2019**, *10*, 736.

45 Lin, X.; Zhang, L.; Duan, B. Polyphenol-mediated chitin self-assembly for constructing a fully naturally resourced hydrogel with high strength and toughness. *Mater. Horiz.* **2021**, *8*, 2503.

46 Fang, Y.; Mu, L.; Lu, Y.; Wu, S.; Zhong, Z.; Ye, Q.; Cai, J. Coagulation-independent hemostasis through architecturally programmed chitosan aerogels with dual-crosslinked networks. *Adv. Mater.* **2026**, e23140.

47 Krol, P. Synthesis methods, chemical structures and phase structures of linear polyurethanes. Properties and applications of linear polyurethanes in polyurethane elastomers, copolymers and ionomers. *Prog. Mater. Sci.* **2007**, *52*, 915–1015.

48 Liu, L.; Lu, J.; Zhang, Y.; Liang, H.; Liang, D.; Jiang, J.; Lu, Q.; Quirino, R. L.; Zhang, C. Thermosetting polyurethanes prepared with the aid of a fully bio-based emulsifier with high bio-content, high solid content, and superior mechanical properties. *Green Chem.* **2019**, *21*, 526–537.

49 Li, S.; Lin, X.; Gong, S. High strength, high stiffness and toughness, defect-tolerant waterborne polyurethane with healing and antibacterial abilities. *J. Polym. Sci.* **2024**, *62*, 388–400.

50 Huang, Y.; Duan, X.; Wei, Q.; Lieber, C. M. Directed assembly of one-dimensional nanostructures into functional networks. *Science* **2001**, *291*, 630–633.

51 Gurunathan, T.; Chung, J. S. Physicochemical Properties of Amino-silane-terminated vegetable oil-based waterborne polyurethane nanocomposites. *ACS Sustain. Chem. Eng.* **2016**, *4*, 4645–4653.

52 Gaddam, S. K.; Kutcherlapati, S. N. R.; Palanisamy, A. Self-cross-linkable anionic waterborne polyurethane–silanol dispersions from cottonseed-oil-based phosphorylated polyol as ionic soft segment. *ACS Sustain. Chem. Eng.* **2017**, *5*, 6447–6455.

53 Li, X.; Cheng, N.; Lin, Y.; Zhang, B.; Yang, Y.; Qu, C.; Wang, X.; Yu, J.; Ding, B. Articular cartilage inspired ultra-strong and tough bio-based polyurethane nanofiber membranes. *Angew. Chem. Int. Ed.* **2025**, *64*, e202505034.

54 Wang, D.; Wang, Z.; Ren, S.; Xu, J.; Wang, C.; Hu, P.; Fu, J. Molecular engineering of a colorless, extremely tough, superiorly self-recoverable, and healable poly(urethane-urea) elastomer for impact-resistant applications. *Mater. Horiz.* **2021**, *8*, 2238–2250.

55 Jang, S.; Go, E. M.; Kim, J.-K.; Kwak, S. K.; Jin, J. Optically transparent, ultra-tough, aerosol-sprayable, waterborne polyurethane composite reinforced with natural polymer nanofibers. *Compos. Part-B Eng.* **2022**, *247*, 110353.

56 Yao, Y.; Xu, Z.; Liu, B.; Xiao, M.; Yang, J.; Liu, W. Multiple H-bonding chain extender-based ultrastiff thermoplastic polyurethanes with autonomous self-healability, solvent-free adhesiveness, and AIE fluorescence. *Adv. Funct. Mater.* **2020**, 2006944.

57 Gomez-Lopez, A.; Panchireddy, S.; Grignard, B.; Calvo, I.; Jerome, C.; Detrembleur, C.; Sardon, H. Poly(hydroxyurethane) adhesives and coatings: state-of-the-art and future directions. *ACS Sustain. Chem. Eng.* **2021**, *9*, 9541–9562.

58 Wang, D.; Yang, K.; Cheng, S.; Fu, M.; Wang, Z.; Li, L.; Zhang, X.; Han, L.; Ren, W.; Yang, F.; Zhang, R. Harsh environment resistible and recyclable thermoplastic polyurea adhesive based on stable and density hydrogen bonds. *Chem. Eng. J.* **2024**, *482*, 148663.

59 Chen, W. C.; Chien, H. W. Enhancing the antibacterial property of chitosan through synergistic alkylation and chlorination. *Int. J. Biol. Macromol.* **2022**, *217*, 321–329.

https://doi.org/10.1007/s10118-026-3773-8